EXPERIMENTAL STUDY ON SCALAR SOURCE ESTIMATION BY ACTIVE LEARNING ENHANCED PHYSICS-INFORMED NEURAL NETWORK

Yanda Tan
Department of Mechanical Engineering
The University of Tokyo
7-3-1 Hongo, Bunkyo-ku, Tokyo, Japan
tanyanda@iis.u-tokyo.ac.jp

Ming Liu
Center for Research on
Innovative Simulation Software
Institute of Industrial Science
The University of Tokyo
4-6-1 Komaba, Meguro-ku, Tokyo, Japan
liuming@iis.u-tokyo.ac.jp

Yosuke Hasegawa
Center for Research on Innovative Simulation Software
Institute of Industrial Science
The University of Tokyo
4-6-1 Komaba, Meguro-ku, Tokyo, Japan
ysk@iis.u-tokyo.ac.jp

ABSTRACT

The efficient localization of scalar sources is critical for environmental monitoring and disaster assessment, which requires the reconstruction of dispersive scalar fields from limited measurements. Although various algorithms have been proposed, most studies rely on numerical simulations, while experimental validations remain limited. In this study, a scalar source estimation framework combining Active Learning (AL) and Physics-Informed Neural Networks (PINN) is developed and implemented in a wind-tunnel experiment. The PINN reconstructs the scalar field from sparse measurements obtained by a mobile robot, while AL guides the sequential sensor placement. The results demonstrate that the framework can successfully identify the source online. Furthermore, the performance strongly depends on the stopping criterion and the amount of initial sensing information, highlighting the importance of appropriate stopping criteria and sensor initialization for reliable and efficient localization.

1 INTRODUCTION

Rapid and reliable localization of pollutant or hazardous gas sources, together with dispersion characterization, is essential for environmental monitoring, disaster response, and industrial leakage control (Liu and Zhai, 2007). Mobile robots provide particular advantages in such scenarios where human access is restricted or unsafe (Wang et al., 2019).

Various approaches have been proposed for scalar source estimation, and they are usually categorized by analytical method (Liu and Zhai, 2007), inverse optimization method (Gorelick et al., 1983; Mahar and Datta, 1997), and heuristic methods (Liu and Zhai, 2007). The latter two are more attractive because of their accuracy and robustness, while the computational cost can also be high. Machine learning techniques, typified by physics-informed neural networks (PINNs) (Raissi et al., 2019; Karniadakis et al., 2021), have emerged as a promising framework, enabling efficient reconstruction of flow and associated scalar fields.

The reconstruction of scalar fields and the identification of the resultant sources strongly depend on the number and placement of the sensors. Therefore, it is critical to determine optimal sensor locations, and numerous strategies have been proposed, such as information-theoretic criteria (Settles, 2012) and heuristic exploration approaches. These methods aim to maximize information gain with minimizing sampling effort, yet practical constraints often limit their effectiveness in real environments.

So far, most prior studies have been confined to numerical simulations (Cerizza et al., 2016; Wang et al., 2019), while the validation in experimental systems is relatively rare. To this end, we implement a PINN-based scalar source estimation framework enhanced with an active learning (AL) strategy in a wind-tunnel experiment with a mobile robot.

2 METHODOLOGY

2.1 Problem description

We consider the advection–diffusion of a scalar field c from a source in a two-dimensional turbulent flow. As illustrated in Fig. 1, a diagonal flow is imposed in a domain of 3.0m × 2.0m, with the inlet and outlet located at (0m, [1.5,1.8]m) and (3.0m, [0.2,0.5]m), respectively. A Dirichlet boundary condition of $c = 0$ is prescribed at the inlet, while an outflow condition is applied at the outlet. Zero-gradient conditions are imposed on the remaining walls. Sensors are positioned downstream of the scalar source, and their measurements are adopted to estimate the source location. In this study, the velocity field is assumed to be known. The scalar field is reconstructed using PINN with measured results, and subsequent sensor locations are determined adaptively through active learning.

2.2 Physics-Informed Neural Network (PINN)

By introducing the Reynolds-Averaged assumption, the scalar transport is formulated by the steady advection–diffusion equation

$$\mathbf{u} \cdot \nabla c = \nabla \cdot [(D_{\text{eff}}) \nabla c] + \phi, \tag{1}$$

where the velocity field $\mathbf{u}$ is predetermined from a RANS simulation and used in the scalar equation. The effective diffusivity D_{eff} consists of molecular diffusivity D_m and the eddy diffusivity $D_t = \frac{\nu_t}{Sc_t}$ where the eddy viscosity ν_t is obtained from RANS simulations with $Sc_t = 1$.

A PINN is adopted to reconstruct the scalar field from sparse measurements, and the cost functional is defined as

$$J = \alpha L_m + \beta L_{pde} + \gamma L_{bc} + \delta L_{pen}, \tag{2}$$

where L_m, L_{pde}, L_{bc}, and L_{pen} denote losses due to the measurement residual, the governing equation, the boundary condition, and the regularization, respectively, and α, β, γ, and δ are corresponding weighting parameters. The weighting coefficients are adaptively adjusted during training to balance the magnitudes of each term, allowing the model to remain sensitive to newly added measurements in the active learning iterations while preserving physical consistency.

The network outputs both the scalar field $c(\mathbf{x})$ and the estimated possibility of the source distribution $\phi(\mathbf{x})$. Then, the source location is identified as the position with the maximum ϕ. The network consists of three hidden layers with 30 neurons and is trained sequentially using Adam followed by L-BFGS.

2.3 Active learning for sensor placement

To enhance source localization with sparse measurements, an Active Learning (AL) strategy is adopted and combined with PINN. AL adaptively selects the next sensor location according to the acquisition function,

$$acq(\mathbf{x}) = \left(\alpha_{\text{acq}} L_{pde}(\mathbf{x}) + \beta_{\text{acq}} \hat{\phi}(\mathbf{x})\right) f_{exc}(\mathbf{x}), \tag{3}$$

where $f_{exc}(\mathbf{x})$ is a binary coefficient that is set as 0 inside exclusion zones and 1 elsewhere so as to avoid redundant sampling near existing sensors. The exclusion zone is defined as an ellipse centered at a sensor, with the major axis aligned to the local flow direction. The axes lengths of the ellipse are given by

$$a_k(\mathbf{x}^m) = \min\left(\max\left(\alpha \frac{\tilde{c}_{\text{ref}}}{|\partial \tilde{c}/\partial x_{\text{flow}}|_{\mathbf{x}^m}} e^{-\lambda k}, a_{\min}\right), a_{\max}\right), \tag{4}$$

$$b_k(\mathbf{x}^m) = \min\left(\max\left(\beta \frac{\tilde{c}_{\text{ref}}}{|\partial \tilde{c}/\partial x_n|_{\mathbf{x}^m}} e^{-\lambda k}, b_{\min}\right), b_{\max}\right), \tag{5}$$

where k denotes iteration index, and the exponential term $e^{-\lambda k}$ introduces a dynamic decay so that the exclusion zones gradually shrink as the AL proceeds. Here, $\tilde{c}_{\text{ref}} = \sigma(\tilde{c}(\mathbf{x}))$ is the standard deviation of the estimated concentration field, which is updated at each AL round. The terms $\partial \tilde{c}/\partial x_{\text{flow}}$ and $\partial \tilde{c}/\partial x_n$ represent the concentration gradients along and perpendicular to the local flow direction, respectively. The clipping operator ensures that the ellipse sizes remain within predefined bounds $[a_{\min}, a_{\max}]$ and $[b_{\min}, b_{\max}]$, preventing extreme shapes.

The sensor is placed at the location with the maximum $acq(\mathbf{x})$, and the PINN is retrained with the newly acquired measurement for 2000 iterations at each AL step. This process is iteratively performed until the difference between the estimated source locations in consecutive iterations satisfies a predefined convergence criterion, i.e., a single-step or a double-step stopping criterion.

2.4 Stopping criteria and performance indices

The source localization is regarded as converged when the change between consecutive predictions satisfies

$$\|\mathbf{x}_k - \mathbf{x}_{k-1}\| < \Delta_{\text{stop}}, \tag{6}$$

where $\mathbf{x}_k$ denotes the predicted source location at the k-th AL iteration. This is referred to as the single-step stopping criterion. In addition, a double-step stopping criterion is also considered, in which convergence is stated only when two consecutive changes both satisfy

$$\|\mathbf{x}_k - \mathbf{x}_{k-1}\| < \Delta_{\text{stop}} \quad \text{and} \quad \|\mathbf{x}_{k+1} - \mathbf{x}_k\| < \Delta_{\text{stop}}. \tag{7}$$

This introduces temporal consistency and improves robustness against noise and prediction oscillations.

The accuracy for source localization is evaluated using the distance of maxima (DoM), which measures the distance between the predicted and true source locations. To further characterize the robustness, a success rate is introduced. A trial is regarded as success when the predicted source is within a certain range around the true source, i.e., 20 cm. For each configuration, 10 trails are performed, and the success rate among the 10 trails is calculated accordingly.

To assess the time consumption of the present method, an equivalent operating time is defined as

$$T_{\text{eq}} = \frac{L}{v} + N t_{\text{sample}} + k t_{\text{train}}, \tag{8}$$

where L is the total robot path length, v the robot speed, N the total number of sensing points, t_{sample} the single sensing time, k the number of active-learning iterations, and t_{train} the training time per iteration. In the present study, they are set as $v = 0.05$ m/s, $t_{\text{sample}} = 100$ s, and $t_{\text{train}} \approx 280$ s. The defined equivalent operating time allows for a fair comparison among various configurations by combining the time consumptions for the robot motion, the sensing, and the model training.

3 EXPERIMENTAL SETUP

3.1 Wind tunnel system

Experiments were conducted in a wind tunnel with dimensions of $3\,\text{m} \times 2\,\text{m} \times 0.25\,\text{m}$, as shown in Fig. 2. The flow is assumed as two-dimensional, since the length in z-direction is relatively small compared to the other two directions. The inflow from the inlet is supplied by an air compressor with a fixed velocity of $0.8\,\text{m/s}$. This corresponds to $Re \approx 10582$ where the half inlet width is taken as the reference length scale. The saturated ethanol vapor is released from a source location of (0.1m, 1.75m), slightly downstream of the inlet as shown in Fig. 1, with a volumetric flow rate of 10 L/min.

3.2 Mobile robots

A mobile robot equipped with an ethanol sensor is used to measure the scalar concentration at target sensor locations. A camera-based positioning system is mounted above the wind tunnel to allow for real-time tracking. The platform integrates an Arduino controller, motors, batteries, and Wi-Fi communication, while optical markers on the top plate allow position tracking by the camera. During the experiment, the mobile robot is dynamically moved to the next sensor location determined by AL. The schematic of the experimental system is illustrated in Fig. 2.

4 RESULTS

4.1 Case summary

All the cases investigated in the present study are summarized in Table 1. As shown in the first column of Table 1, the Case ID is expressed by the stopping criterion, the stopping threshold, and the number of initial sensors. With the present experimental configurations, the influence of these three factors on the source localization results is studied. For each case, 10 repeated runs are conducted to ensure statistical reliability. The mean distance of maxima (DoM) and the mean equivalent time are computed as the averages over these runs. The error bars represent one standard deviation from the mean, reflecting the variability of the results across repeated trials.

Figure 3 presents the example of a successful localization case, i.e., Case D-T15-N5, with double-step criterion, Δ_{stop} = 15 cm, and $n_{\mathrm{init}} = 5$. Figure 3(a) shows the robot route together with the consecutive sensor placement dertermined by the active learning, while Figure 3(b) illustrates the evolution of the predicted source location in each AL iteration until convergence, and the labeled number denotes the iteration index.

4.2 Comparison of single- and double-step stopping criteria

Figure 4 plots the comparison of the performance indices, i.e., DoM, T_{eq}, and success rate, between the single-step and double-step stopping criterion with two stopping thresholds for cases S-T09-N5, D-T09-N5, S-T12-N5, and D-T12-N5. Under a strict threshold, i.e., $\Delta_{\mathrm{stop}} = 9$ cm, the performance indices of DoM and success rate using the double-step strategy is comparable to that using the single-step strategy, while the operating time becomes longer. The variations of the DoM and the success rate are also of a similar level between the single-step and the double-step strategies. By comparison, the double-step strategy exhibits a improvement in both reducing the DoM and increasing the success rate under a more relaxed threshold, i.e., $\Delta_{\mathrm{stop}} = 12$ cm, while it is at the cost of longer operating time. Moreover, the variations of the DoM and the operating time are also reduced when using the double-step strategy compared to the single-strategy. The above comparison show that the double-strategy can improve both the accuracy and the robustness of the present algorithm with a relaxed threshold, while a strict threshold can deteriorate the improvement.

4.3 Influence of stopping thresholds

In this subsection, we fix the double-step strategy and focus on the influence of the stopping thresholds by cases D-T12-N5, D-T15-N5, D-T18-N5, and D-T21-N5, where the stopping threshold is systematically increased from 12 cm to 21 cm. The experimental results are plotted in Fig. 5. Generally, as the stopping threshold increases, the operating time gradually reduces. Regarding the Dom and the success rate, the best estimation performance, i.e., the minimum DoM of 10.1 cm, and the maximum success rate of 100%, is achieved under $\Delta_{\mathrm{stop}} = 15$ cm. These results indicate that excessively relaxing the stopping threshold leads to early termination without sufficient accuracy, whereas overly strict thresholds increase computational cost without further performance gains. Under the present conditions, the threshold of $\Delta_{\mathrm{stop}} = 15$ cm provides a balance among accuracy, robustness, and efficiency.

4.4 Influence of initial sensor configurations

The quantity and spatial distribution of initial sensors play a critical role in determining the amount of information available for PINN learning at the early stage. To examine this effect, three values of the number of the initial sensors, i.e.,n_{init} = 3, 5, and 8 are considered using the double-step strategy with $\Delta_{\mathrm{stop}} = 15$ cm. As illustrated in Fig. 1, the corresponding candidate sensor locations are marked with different symbols, representing the configurations D-T15-N3, D-T15-N5, and D-T15-N8, respectively.The experimental results with different number of initial sensors are plotted in Fig. 6. When the number of the initial sensors is increased from 3 to 5, both the DoM and the operating time reduces, and the success rate increases. However, these three performance indices hardly changes as n_{init} = 8 is further increased to 8. Although the averaged performance indices is not improved from n_{init} = 5 to 8, their variations are still be reduced. These results suggest that 5 initial sensors are sufficient to achieve a well source localization accuracy, while further increase in the number of initial sensors does not result in a performance improvement.

5 CONCLUSIONS

In this study, a scalar source localization framework combining Physics-Informed Neural Networks and active learning is developed and validated through wind-tunnel experiments with a mobile robot. Unlike previous studies focusing mainly on algorithm design, this work emphasizes how physical settings and stopping criteria influence overall performance.

The results show that the proposed PINN framework with active learning can successfully identify the source with limited measurements with proper configurations. The influences of the stopping criterion, the stopping threshold, and the initial sensor configuration are systematically investigated in the present study. The single-step criterion cannot ensure stable convergence, whereas the double-step criterion provides more reliable localization. Under the double-step criterion, both overly strict and overly loose thresholds degrade performance, while a moderate threshold achieves the best balance between accuracy and efficiency. Sufficient initial sensor information is essential for stable PINN learning, whereas overly sparse sensor configurations may lead to unsuccessful localization and large prediction fluctuations.

Despite these findings, the present study is limited to a finite set of experimental configurations. More fundamentally, the effectiveness of sensing is not determined solely by the number of sensors, but by the information they provide within a given flow and concentration field. Understanding how sensing locations interact with underlying physical structures remains an open question. Future work will therefore focus on exploring information-driven sensing strategies under more diverse flow conditions, aiming to establish more general principles for sensor placement and active learning design.

REFERENCES

Liu, X., and Zhai, Z., 2007, "Inverse modeling methods for indoor airborne pollutant tracking: Literature review and fundamentals," *Indoor Air*, Vol. 17, No. 6, pp. 419–438.

Gorelick, S. M., Evans, B., and Remson, I., 1983, "Identifying sources of groundwater pollution: An optimization approach," *Water Resources Research*, Vol. 19, No. 3, pp. 779–790.

Mahar, P. S., and Datta, B., 1997, "Optimal monitoring network and groundwater-pollution source identification," *Journal of Water Resources Planning and Management*, Vol. 123, No. 4, pp. 199–207.

Raissi, M., Perdikaris, P., and Karniadakis, G. E., 2019, "Physics-informed neural networks: A deep learning framework for solving forward and inverse problems involving nonlinear PDEs," *Journal of Computational Physics*, Vol. 378, pp. 686–707.

Karniadakis, G. E., Kevrekidis, I. G., Lu, L., Perdikaris, P., Wang, S., and Yang, L., 2021, "Physics-informed machine learning," *Nature Reviews Physics*, Vol. 3, pp. 422–440.

Cohn, D., Ghahramani, Z., and Jordan, M. I., 1996, "Active learning with statistical models," *Journal of Artificial Intelligence Research*, Vol. 4, pp. 129–145.

Cerizza, D., Sekiguchi, W., Tsukahara, T., Zaki, T. A., and Hasegawa, Y., 2016, "Reconstruction of scalar source intensity based on sensor signal in turbulent channel flow," *Flow, Turbulence and Combustion*, Vol. 97, No. 4, pp. 1211–1233.

Settles, B., 2012, *Active Learning*, Synthesis Lectures on Artificial Intelligence and Machine Learning, Morgan & Claypool, Vol. 6, No. 1, pp. 1–114.

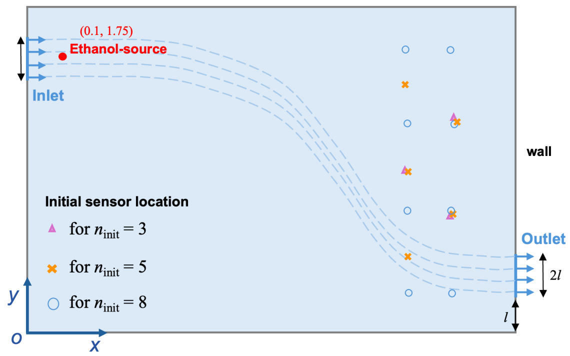

Figure 1: Schematic of the wind-tunnel setup. As the initial sensor configurations, for $n_{\text{init}} = 3$ (D-T15-N3): $(2.7, 1.34)$, $(2.5, 1.00)$, $(2.7, 0.67)$; For $n_{\text{init}} = 5$ (D-T15-N5): $(2.5, 0.5)$, $(2.5, 1.0)$, $(2.5, 1.5)$, $(2.7, 0.67)$, $(2.7, 1.34)$; For $n_{\text{init}} = 8$ (D-T15-N8): $x \in 2.5, 2.7$, $y \in 0.25, 0.75, 1.25, 1.75$.

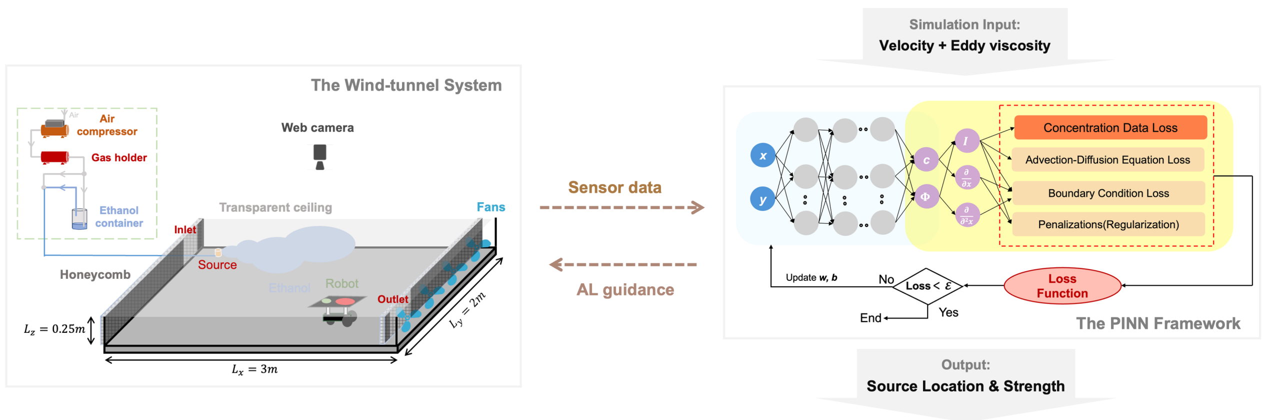

Figure 2: Schematic of the wind-tunnel experiment with a mobile robot.

Table 1: Case definitions for different stopping criteria and initial sensor settings.

Case ID	Stopping criterion	Δ_{stop} (cm)	n_{init}
S-T09-N5	single-step	9	5
S-T12-N5	single-step	12	5
D-T09-N5	double-step	9	5
D-T12-N5	double-step	12	5
D-T15-N5	double-step	15	5
D-T18-N5	double-step	18	5
D-T21-N5	double-step	21	5
D-T15-N3	double-step	15	3
D-T15-N8	double-step	15	8

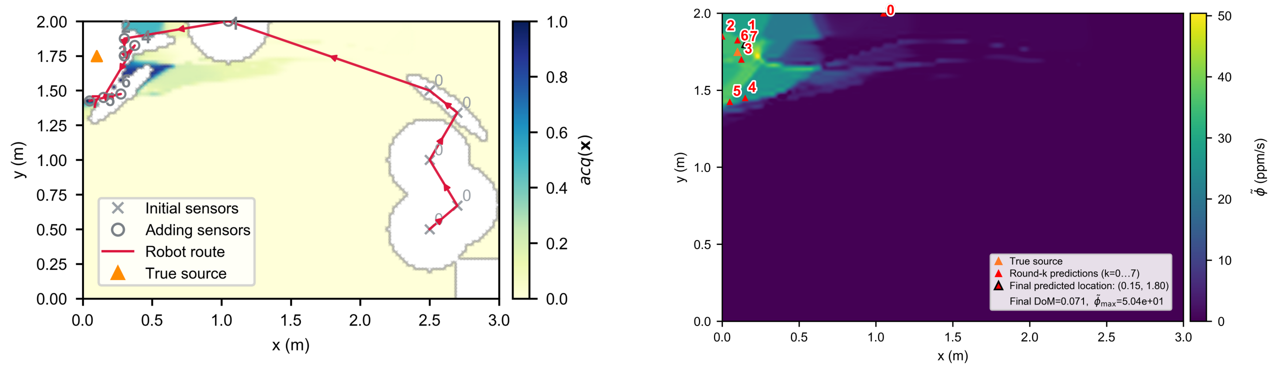

(a) Robot route and AL sensor placement *(b)* Source prediction evolution

Figure 3: One successful D-T15-N5 case (double-step criterion with $\Delta_{\mathrm{stop}} = 15\mathrm{cm}$, $n_{\mathrm{init}} = 5$) localization example. Number k denotes the active-learning iteration: in (a), 0 indicates initial sensors and k indicates the sensor added at step k; in (b), k indicates the predicted source after the k-th AL iteration.

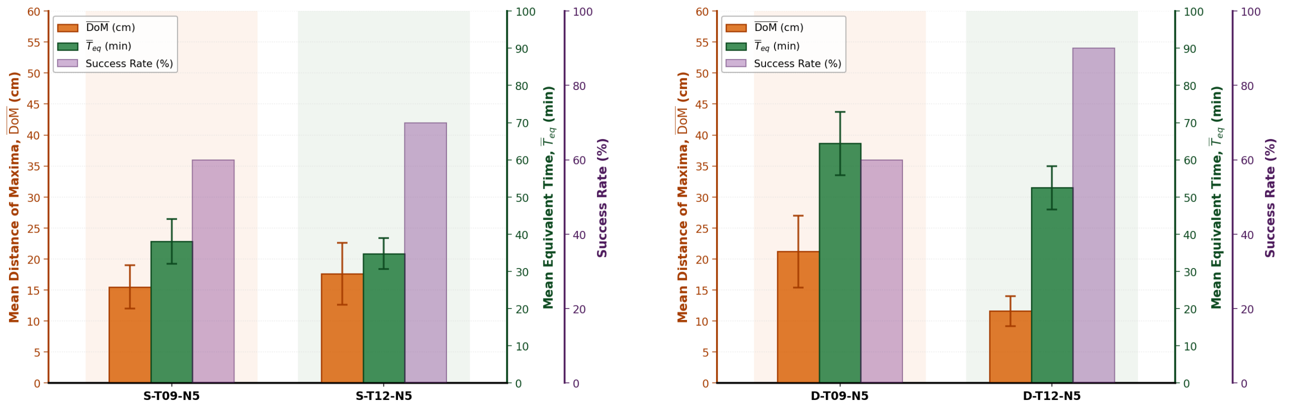

(a) $\Delta_{\mathrm{stop}} = 9\,\mathrm{cm}$ *(b)* $\Delta_{\mathrm{stop}} = 12\,\mathrm{cm}$

Figure 4: Comparison of experimental results between single-step and double-step stopping criteria under the threshold of (a) $\Delta_{\mathrm{stop}} = 9\,\mathrm{cm}$ and (b) $\Delta_{\mathrm{stop}} = 12\,\mathrm{cm}$ for cases S-T09-N5, D-T09-N5, S-T12-N5, and D-T12-N5.

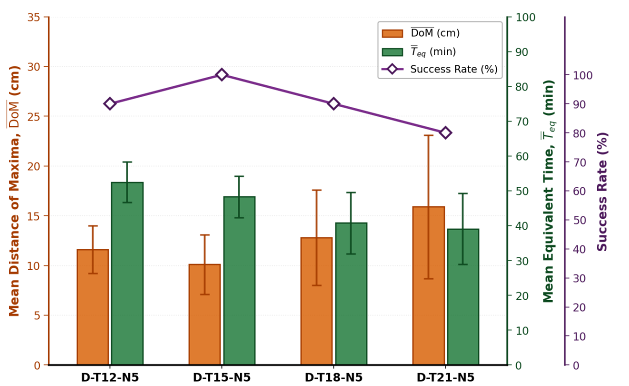

Figure 5: Influence of double-step stopping thresholds for cases D-T12-N5, D-T15-N5, D-T18-N5, and D-T21-N5.

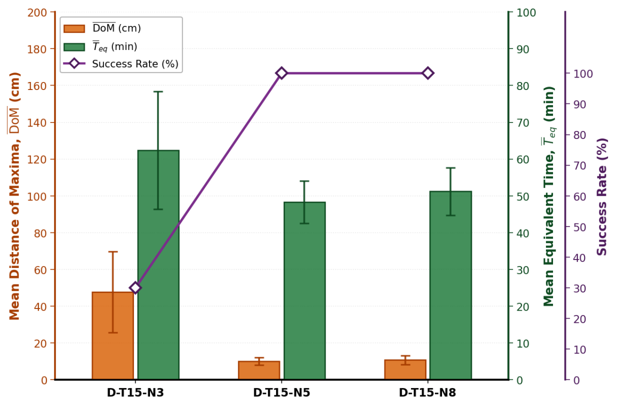

Figure 6: Influence of initial sensor configurations for cases D-T15-N3, D-T15-N5, and D-T15-N8.